Potts model solver based on hybrid physical and digital architecture

Kensuke Inaba (kensuke.inaba.yg@hco.ntt.co.jp)
NTT Corporation https://orcid.org/0000-0003-1227-4925
Takahiro Inagaki
NTT Corporation
Koji Igarashi
Osaka University
Shoko Utsunomiya
National Institute of Informatics
Toshimori Honjo
NTT Corporation
Takuya Ikuta
NTT Corporation
Koji Enbutsu
NTT Corporation
Takeshi Umeki
NTT Corporation
Ryoichi Kasahara
NTT Corporation
Kyo Inoue
Osaka University
Yoshihisa Yamamoto
NTT Research Inc.
Hiroki Takesue
NTT Corporation

Article

Keywords: Potts model, solver, physical and digital architectures, integer optimization, optical parametric oscillators

Posted Date: May 10th, 2021

DOI: https://doi.org/10.21203/rs.3.rs-464366/v1

Version of Record: A version of this preprint was published at Communications Physics on May 31st, 2022. See the published version at https://doi.org/10.1038/s42005-022-00908-0.

Potts model solver based on hybrid physical and digital architecture

Abstract

The Potts model describes Ising-model-like interacting spin systems with multivalued spin component, and ground-state search problems of the Potts model can be efficiently mapped onto various integer optimization problems thanks to the rich expression of the multivalued spins. Here, we demonstrate a solver of this model based on hybrid computation using physical and digital architectures, wherein a digital computer updates the interaction matrices in the iterative calculations of the physical Ising-model solvers. This update of interactions corresponds to learning from the Ising solutions, which allows us to save resources when embedding a problem in a physical system. We experimentally solved integer optimization problems (graph coloring and graph clustering) with this hybrid architecture in which the physical solver consisted of coupled degenerate optical parametric oscillators.

Introduction

The connection between searches for the ground-states (GS) of physical systems and optimization problems has activated research and development into new types of computation [1]. The realization of such architectures has been led off by the Ising-model solvers [2-9]. These physical-model-solver architectures have solved certain problems much faster than conventional digital architectures such as a CPU [10-13]. Here, embedding of problems in a physical model sometimes requires an overhead of resources, which can be large enough to be a computational bottleneck. However, the embedding overhead can be reduced by choosing more appreciate physical model as a solver instead of the Ising model [14-16].

The Potts model is a fundamental model describing various physical and mathematical problems [18], such as those of percolation theory [19]. This model is a generalization of the Ising model to multivalued spins; its Hamiltonian is given by

$$\mathrm{H}_{\mathrm{Potts}} = \sum_{ij} J_{ij}\,\delta(S_i, S_j), \qquad (1)$$

where $S_i = \{0,1,2,\dots,M-1\}$ is an M-component spin on i-th node of the model, where $i = \{1,2,3,\dots,N\}$, and $\delta(a,b)$ is the Kronecker delta function. Since multivalued spins naturally express integers, various integer optimization problems can be straightforwardly mapped onto GS search problems based of this model [18]. For example, graph coloring can be described as a Potts model with a smaller Hilbert space than that of the standard Ising model [20]. In the standard Ising-model mapping, M colors in each node are represented as M Ising spins [20]; thus, the size of its Hilbert space is 2^{NM}, which is larger than that of the original M-color problem i.e., M^N $\left(= 2^{N \log_2 M}\right)$. The Ising Hamiltonian has constraint terms to reduce the size of the enlarged space to that of the original problem, while the Potts model without constraint Hamiltonian has the same size as that of the original. Thus the Potts model mapping allows us to avoid the embedding overhead. [The details are discussed in Supplementary Note 1 in Supplementary Information (SI).] On the other hand, there are several challenges to realizing a physical Potts solver, namely, the implementations of multivalued spins and interactions described by a Kronecker delta within physical systems. It has been proposed that a few physical systems can be used to solve specific Potts problems [14,15].

In this study, we demonstrated a scheme to solve the Potts problem by using a hybrid architecture of a physical Ising-model solver and digital processing (Fig. 1a). The Potts problem can be approximately solved by iterative calculations of Ising problems with updated interactions evaluated from one-way feedforward connections. This one-way approximation causes the degradation in solution accuracy, which can be reduced by additional feedback connections. These feedforward and feedback connections are encoded in digital processing, which can be regarded as learning processes in between physical Ising solvers. Hybrid computation enjoy the advantages of physical solvers through the aid of digital computers [21,22]: The physical solver obtains a low energy solution of a complex Ising problem (known to be NP [1]) quickly [10-13], while the digital computer can accurately handle input and output, such as, interactions and energy and also run the learning logic (see Fig. 1a).

We implemented a Potts solver by using a coherent Ising machine (CIM) [5,10,23-25] and a standard CPU (Fig. 1b). The CIM is a physical Ising-model solver based on coupled degenerate optical parametric oscillators

(DOPOs) [23], in which Ising spins are encoded by utilizing the bifurcation transition in each DOPO [23], and the spin-spin couplings are implemented by a measurement feedback scheme [10,25]. Low energy solutions of an Ising model are physically determined as a result of competition between optical gain and loss in coupled oscillators [23]. We experimentally solved two integer optimization problems, i.e., clustering and coloring, on the same graph (see Fig. 2).

Theoretical framework

First, we explain how to map a Potts problem on one involving iterative calculations of Ising models. Given an integer $L \equiv \mathrm{ceil}(\log_2 M)$, a multivalued spin S_i can be written by a set of Ising spins $\sigma_i^{(l)} = \{-1,1\}\,(l = 1,2,\dots,L)$ with a standard binary representation, as $S_i = \sum_{l=1}^{L} \frac{1+\sigma_i^{(l)}}{2}\, 2^{l-1}$. The Hamiltonian in Eq. (1) is rewritten as $\mathrm{H_{Potts}} = \sum_{ij} J_{ij} \prod_{l=1}^{L} \frac{1+\sigma_i^{(l)}\sigma_j^{(l)}}{2}$, where the delta functional Potts interaction is transformed into multibody Ising-spin interactions $\prod_{l=1}^{L} \frac{1+\sigma_i^{(l)}\sigma_j^{(l)}}{2}$. This complicated interaction can be simplified by decomposing it into sets of two-body interactions $\sigma_i^{(l)}\sigma_j^{(l)}$ on L Ising problems with one-way feedforward connections: $\mathrm{H}_{\mathrm{Ising}}^{(l)} = \sum_{ij} J_{ij}^{(l)}\, \sigma_i^{(l)}\sigma_j^{(l)}$. Here, l means an iteration number and is called stage. The interaction matrix $J_{ij}^{(l+1)}$ is determined recursively from an iteration $J_{ij}^{(l)}$ and a solution $s_i^{(l)}$ of the previous stage:

$$J_{ij}^{(l+1)} = \frac{1 + s_i^{(l)} s_j^{(l)}}{2} J_{ij}^{(l)}, \qquad (2)$$

where the initial Ising interactions are the same as the original Potts interactions $J_{ij}^{(1)} = J_{ij}$.

Figure 1a illustrates the framework of the Potts solver based on hybrid computation. We repeat operation stages including two parts; the Ising-solver part that obtains a solution $s_j^{(l)}$ for an input $J_{ij}^{(l)}$, and the digital part that calculates $J_{ij}^{(l+1)}$ in Eq. (2). The digital part also calculates the Potts energy defined by $E_{\mathrm{Potts}}^{(l)} = \sum_{ij} J_{ij}\delta(S_i^{(l)}, S_j^{(l)})$, where the Potts spin $S_i^{(l)} = \{0,1,\dots,M^{(l)} - 1\}$, for $M^{(l)} = 2^l$, is given by

$$S_i^{(l)} = S_i^{(l-1)} + \frac{1 + s_i^{(l)}}{2} M^{(l-1)}. \quad (3)$$

From Eq. (2), we can derive two other expressions of Potts energy: $E_{\mathrm{Potts}}^{(l)} = \sum_{ij} J_{ij}^{(l)} \frac{1+s_i^{(l)}s_j^{(l)}}{2}$ and $E_{\mathrm{Potts}}^{(l)} = \sum_{ij} J_{ij}^{(l+1)}$. When $l = L$ (final stage), we obtain a solution $S_i^* (= S_i^{(L)})$ and Potts energy $E_{\mathrm{Potts}}^* (= E_{\mathrm{Potts}}^{(L)})$.

Let us discuss the convergence of the above approximation by considering the energy improvement $\Delta E_{\mathrm{Potts}}^{(l)} \equiv E_{\mathrm{Potts}}^{(l)} - E_{\mathrm{Potts}}^{(l-1)}$. From the above two expressions of $E_{\mathrm{Potts}}^{(l)}$, we can rewrite $\Delta E_{\mathrm{Potts}}^{(l)}$ as $\frac{1}{2}\left(E_{\mathrm{Ising}}^{(l)} - F_{\mathrm{Ising}}^{(l)}\right)$, where $E_{\mathrm{Ising}}^{(l)} = \sum_{ij} J_{ij}^{(l)} s_i^{(l)} s_j^{(l)}$ is the Ising energy of a solution in stage l, and $F_{\mathrm{Ising}}^{(l)} = \sum_{ij} J_{ij}^{(l)}$ is the energy of ferromagnetic (FM) states in stage l (e.g., FM means $s_i^{(l)} = -1$ for all i). We can conclude that $E_{\mathrm{Potts}}^{(l)}$ decreases in an iteration l, if each stage yields a lower-energy solution than the FM states: $E_{\mathrm{Ising}}^{(l)} < F_{\mathrm{Ising}}^{(l)}$. Note that the FM states are trivially obtained for any $J_{ij}^{(l)}$. Meanwhile, a convergence condition $\Delta E_{\mathrm{Potts}}^{(l)} = 0$ is satisfied when the obtained solution is same as the FM state. Equation (3) indicates the convergence of a change in spins $S_i^{(l)} = S_i^{(l-1)}$ for the FM solutions (see Method for details).

A low-energy solution S_i^* is, however, not assured to be the GS of the original Potts model. This problem is mainly attributed to the one-way feedforward connection of $J_{ij}^{(l)}$ described by Eq. (2): Namely, as l increases, the interaction matrix and graph are divided up into more and more submatrices and subgraphs, as illustrated in Fig. 1a. The loss of information from J_{ij} and the reduction of the graph degrade the solution accuracy. Such errors can be circumvented by implementing two kinds of feedback: One is recurrent Potts-problem feedback with a new (learned) interaction matrix J_{ij}^{new} (long arrow in Fig. 1a). The other one is digital feedback: Namely, in each digital operation, $J_{ij}^{(l)}$ and $S_i^{(l)}$ are modified to improve Potts energy $E_{\mathrm{Potts}}^{(l)}$(rounded arrows in Fig. 1a). The simplest example of digital feedback is filtering: For $\Delta E_{\mathrm{Potts}}^{(l)} > 0$, we can filter out a bad solution without additional calculations by choosing a better solution in the previous stage. In what follows, we experimentally demonstrate that heuristic feedback algorithms improved clearly the performance of the Potts solver.

Finally, we generalize $J_{ij}^{(l)}$ defined in Eq. (2) to use the feedback algorithms. For convenience, we introduce a weight matrix $W_{ij}^{(l)}$ defined by $W_{ij}^{(l+1)} = \delta(S_i^{(l)}, S_j^{(l)})$, which is a more general form i.e., $J_{ij}^{(l)} = W_{ij}^{(l)} J_{ij}$ than Eq. (2). In summary, weights for interactions $W_{ij}^{(l)}$ are "learned" from the solution of the Ising solvers in each stage so as to decrease the Potts energy. This framework can be regarded as the artificial-neural-network-like algorithm using a physical Ising solver, where decrease in the cost energy function (Potts energy) is assured if the solver can find a low energy Ising solution. Note that this property of convergence may allow us to utilize the advantages of physical solvers that can find low energy solutions quickly.

Results

Graph clustering

We solved a graph clustering problem, which is a task to find the best grouping of nodes. This problem is widely used in various fields, such as community detection in social [26] and biological networks [27-28]. Modularity Q is a good measure for graph clustering problems [29], and a task to maximize Q can be directly mapped onto a search for the GS of the Potts model in Eq. (1) [30]. A multivalued spin S_i identifies a group number to which i-th node belongs. The interaction matrix for this problem is defined as $J_{ij} \equiv B_i B_j - CA_{ij}$, where A_{ij} is the adjacency matrix, $B_i = \sum_j A_{ij}$, and $C = \sum_i B_i$. The Potts energy is related to $Q = -\frac{E_{\text{Potts}}}{C^2}$. There is room to study on the definition of J_{ij} [31], but it is beyond the scope of this paper. Competition between antiferromagnetic (AFM) and FM correlations (namely, a positive $B_i B_j$ and negative $-CA_{ij}$ in J_{ij}, respectively) is the intrinsic difficulty of this problem. Although the number of groups is not given, an optimized M is spontaneously obtained through such FM-AFM competition as discussed below.

We solved a clustering problem on the graph shown in Fig. 2, originating from the prefectures of Japan and has $N = 47$ nodes and $N_{\text{edge}} = 92$ edges. The physical solver used here was a CIM implemented with fully-connectable 512 nodes (see Method and Fig. 1b), in which 470 nodes were used in parallel. It has been demonstrated that, if J_{ij} is a dense matrix, a CIM shows better performance than the standard CPU with simulated annealing [10] and the D-wave system [32]. This suggests that a CIM is appropriate for clustering problems in which J_{ij} is dense owing to a term of $B_i B_j$ with $B_i \neq 0$.

Each CIM calculation took 500 μs (100 5 μs steps), and each digital part took about 30 μs or less. However, the current setup used a slow serial communication interface, and the data transfer of $J_{ij}^{(l)}$ between the CIM and CPU took a few seconds. This bottleneck can be removed by coding the J_{ij}-update logic in FPGA modules (see Method).

Figure 3a-d shows the evolutions of 47 DOPOs during 100 operation steps (circulations in a cavity) in four stages ($l = 1,2,3,$ and 4). Positive (negative) DOPO amplitudes represent up (down) Ising spins. The black lines in Fig. 3e show the change in modularity Q and number of groups M in the same operation steps as those in Fig. 3a-d. For $l = 1$ and 2, the DOPO amplitudes show that AFM states appear after several tens of steps (Fig. 3a and b). As a result, each group split up in two, and M doubled in value (Fig. 3e). At $l = 3$, down-spin DOPOs were the majority (Fig. 3c), indicating that FM correlations were dominant, and M converged to an optimized value of 5 (Fig. 3e). At the beginning of the steps in each stage, Q decreased drastically; while at the end of steps, a CIM selected a higher value of Q than that in the former stage. At $l = 4$, the complete FM state prevailed finally (Fig. 3d), meaning that the stationary condition was satisfied. As mentioned in Method, the obtained grouping with a Q of 0.646 (see Fig. 2) is the same as the best solution obtained by reliable algorithms, such as, the Louvain greedy [33] and the Infomap algorithms [34]. Figure 3f shows that the rate of reaching the highest Q of 1000 trials is about 20%. We can conclude that the FM-AFM competition solved by the CIM provided good groupings with high modularity. See Method and Supplementary Note 6 in SI for details.

We found that two digital feedback algorithms [called domain separation (DS) and group reunion (GR)] improved the performance of our Potts solver. Figure 3e and f (red and blue lines) reveal that they almost doubled the rate of reaching the highest Q. In addition, the highest Q was reached at early stages, so the calculation time was shortened. The digital processing including all of the feedback calculations takes at most 30 μs; they were of the order of $O(N^2)$ (or $O(N_{\text{edge}})$ for sparse A_{ij}).

Domain separation: By detecting magnetic domains (small regions in which spins are in the same), we can recalculate $S_i^{(l)}$ to decrease Potts energy. As illustrated in Fig. 3g, an Ising solver sometimes yields a solution consisting of two or more separated magnetic domains (see Supplementary Note 3 and 4 in SI, and also Ref. [24]). Nodes in separated domains should be different groups owing to the lack of FM correlations

$(-A_{ij})$. Note that the AFM connections (B_iB_j) still remain: Namely, the subgraph consisting of red nodes in Fig. 3g is separated, while the corresponding matrix (red square) is not block diagonal because of the AFM interactions (see Supplementary Note 4 in SI). As depicted in Fig. 3g, by removing the AFM elements from $J_{ij}^{(l)}$, this DS feedback yields a new $J_{ij}^{(l)'}$. As a result, the Potts energy decreases in proportion to the sum of removed AFM elements, i.e., $\sum_{ij}\left[J_{ij}^{(l)'} - J_{ij}^{(l)}\right]$.

Detecting domains and numbering them require a calculation time of $O(N^2)$ or $O(N_{\text{edge}})$. The updated $S_i^{(l)'}$ is determined from the domain number. Now, the number of groups is unlimited, while it was limited to at most 2^l in the case without feedback. As shown in Fig. 3e and f (red lines), DS feedback allows us to reach the best solution with $M = 5$ in the early stages $l < 3$. Thus, the calculation time can be shortened by up to half.

Group reunion: The GR feedback algorithm is schematically shown in Fig. 3h. On the basis of the obtained grouping described by $S_i^{(l)}$, we can calculate the group-group interactions $J_{gg'} \equiv \sum_{ij} J_{ij}\delta(S_i^{(l)}, g)\ \delta(S_j^{(l)}, g')$. As shown in Fig. 3h, this interaction matrix is defined on a new graph with $M^{(l)}$ nodes. The new Potts Hamiltonian $\mathrm{H}_{\text{Potts}} = \sum_{gg'} J_{gg'}\,\delta(S_g, S_{g'})$ describes the task of finding the best way of decreasing the Potts energy by executing reunions of groups. A FM group-group interaction $J_{gg'} < 0$ requires reunion. GR feedback can restore the information lost due to the approximation: Namely, $J_{gg'}$ includes information of the original J_{ij}, whereas a block diagonal $J_{ij}^{(l)}$ loses it.

The Potts problem for a GR task can be efficiently solved by making the following approximation. We unify two groups g_a and g_b for a negative and minimum $J_{g_ag_b}$ without considering the other negative elements, and repeat the same calculations by updating $J_{gg'}$. In each step, the Potts energy is reduced by $2J_{g_ag_b}$. This approximation works very well for small M (see Supplementary Note 5 in SI). The calculation takes $O(N^2)$ or $O(N_{\text{edge}})$ time. GR feedback combined with DS feedback improves the rate of reaching highest Q as shown in Fig. 3e-f.

Graph coloring

Graph coloring is the task of coloring connected nodes [18]. We experimentally solved a four-color problem on the graph in Fig. 2a. We set $L = 2$ for $M = 4$. The interaction matrix was totally AFM $J_{ij} \equiv A_{ij} > 0$, requiring that adjacent nodes be different colors. The four-color theorem [35] assures the existence of a GS with $E^*_{\text{Potts}} = 0$. The CIM operated under the same conditions as described above (see Supplementary Note 7 in SI).

Figure 4a shows the conditional success rates for 50 instances of $J_{ij,k}^{(2)}$ $(k = 1,2,\ldots,50)$, which were obtained as follows: Identical Ising model with J_{ij} in stage one were solved 50 times, then 50 solutions $s_{i,k}^{(1)}$ and 50 Ising models in stage two $J_{ij,k}^{(2)}$ were obtained, where $J_{ij,k}^{(2)} = W_{ij,k}^{(1)}J_{ij}$ and $W_{ij,k}^{(1)} = \delta(s_{i,k}^{(1)}, s_{j,k}^{(1)})$. Then, the conditional success rate was estimated by solving 50 Ising models with $J_{ij,k}^{(2)}$ 100 times. The total success rate averaged over k is about 50%. Fig. 4a shows the energy in stage one $E_{\text{Potts},k}^{(1)}$ for each $s_{i,k}^{(1)}$. Successful and failed instances in stage two are clearly separated irrespective of energy in stage one. This result can be understood from the reduction of the graph in stage two described by $W_{ij,k}^{(1)}A_{ij}$ (see Supplementary Note 3 in SI). Coloring fails with 100% probability regardless of the energy in stage one if the reduced graph in stage two has geometrical frustrations, such as a triangular structure (see Supplementary Note 8 in SI).

Such frustrations can be dissolved by implementing recurrent Potts-problem feedback based on a "learning by mistake" approach. We iteratively execute the Potts solver with $J_{ij}^{\text{new}} = J_{ij}^{\text{old}} + w\,L_{ij}$ and $J_{ij}^{\text{initial}} = w_0\,A_{ij}$, where w and w_0 are weights to control the learning. A feedback matrix is defined by $L_{ij} \equiv W_{ij}^{(2)}A_{ij}$ $(= \{0,1\})$ and is related to the Potts energy as follows $E^*_{\text{Potts}} = \sum_{ij} L_{ij}$. Here, $L_{ij} = 1$ represents adjacent nodes in the same color, while $L_{ij} = 0$ represents those having different colors (or not adjacent). Thus, a finite L_{ij} directly represents a mistake. In the new (learned) Potts problem with J_{ij}^{new}, interactions on the "mistaken edges" are enlarged, and then the pair of nodes on these edges are correctly colored with high priority in stage one. As a result, frustrations caused by the reduction of the graph in stage two are eliminated by learning.

Figure 4b shows how learning affects the success rate for $w = 5, 10, 20,$ and 40 with $w_0 = 40$. Each success rate is obtained by performing 50 trials of a two-stage experiment. In each learning step, L_{ij} is

determined from the worst-case instance with the largest E^*_{potts} in 50 trials. As shown in the Fig. 4b, success rates improved from 50% to over 80% after few learning steps, eventually reaching nearly 100%. A larger w provides fast but unstable improvements (see Supplementary Note 10 of SI).

Figure 4c represents the sum of L_{ij}, corresponding to total counts of mistakes, for four independent learning processes. In each learning process, there was no more than one mistake on the same edge; thus, there was at most four mistakes. The red-colored edges and nodes in Fig. 4c are frequently involved in these mistakes: They can be regarded as the intrinsic origins of frustrations in the graph. By detecting such nodes and edges, the learning process increased the success rate to over 80%.

The present Potts solver can be applied to general coloring problems with M colors [36]: For instance, simple scheduling problems [37] and number puzzles such as Sudoku [38] can be described by graph colorings. It is straightforward to apply the present solver to cases with $M = 2^L$, while a small number of additional nodes (at most N) are required to deal with cases in which $M \neq 2^L$ (see Supplementary Note 2 of SI). For comparison, the usual Ising mapping [20] requires MN nodes (up to N^2). Thus, the Potts solver can save node resource, which will be a benefit for physical solvers having the limitation of node resources.

Discussions and Outlook

We demonstrated a Potts model solver based on a hybrid architecture composed of physical Ising solvers and digital processing. The Potts problem is mapped onto iterative Ising problems with learning of weights for interactions, where convergence is assured if a physical solver can find a low energy Ising solution. We experimentally realized it with a coherent Ising machine (CIM) and a standard CPU (Intel(R) Xeon(R)). We showed that graph coloring and clustering problems can be solved by using simple Ising models (no magnetic fields were used to introduce constraints and there was no need for a large number of spins). The resource overhead for embedding the problem is significantly suppressed. As a tradeoff, iterative calculations with learning (namely, additional computational time) are required. We expect that this additional time is insignificant if the physical solver is fast enough. The cost of the communication between physical and digital systems is an essential problem of hybrid computation, but it can be significantly suppressed by directly coding the learning logic in CIM's measurement feedback systems. In this way, the present hybrid scheme can be used in various applications by utilizing advantages of physical solvers, in particular, CIM and also related algorithms on non-CPU digital devices [39,40].

Methods

Ferromagnetic solutions as a sign of convergence

By considering $\Delta E^{(l)}_{\text{Potts}}$, we can find a convergence condition characterized by FM solutions. Note that there are degenerate FM solutions due to spin inversion symmetry, and the degeneracy d_{FM} increases as $d_{FM} = 2^l$ (or $d_{FM} = 2M^{(l)}$ to put it more precisely) because of the reduction of the graph and interaction matrix. Equation (3) indicates that these FM solutions except for the complete-down state ($s_i^{(l)} = -1$ for all i) cause a (trivial) change in the multivalued spins, which can be reduced to steady spin states $S_i^{(l+1)} = S_i^{(l)}$. Accordingly, we can find another expression for the convergence condition $J_{ij}^{(l+1)} = J_{ij}^{(l)}$.

Experimental set up of CIM

As shown in Fig. 1b, the CIM contains a phase sensitive amplifier (PSA), 1-km fiber ring cavity, and a field-programmable gate array (FPGA) module. We employ a periodically poled lithium niobate (PPLN) waveguide as the PSA, which amplifies lights with only the 0 or π phase components relative to the pump phase as a result of signal-idler degenerate optical parametric amplification [41,42]. These two amplified components express two of the Ising spins. Because the cavity round-trip time is 5 μs and the pump pulse interval is 1 ns, over 5,000 DOPO pulses are generated inside the 1km cavity, from which 512 DOPO pulses are used as artificial Ising spins. The 512 DOPO pulses are mutually coupled by using the measurement and feedback scheme with the FPGA module [10,25]. We can encode an interaction matrix J_{ij} in the FPGA module with eight-bit integers ranging from -128 to 128. For solving the clustering problem, $\max|J_{ij}| \sim C = 2N_{\text{edge}} = 184$, exceeds the maximum range of the FPGA module. Thus, J_{ij} in the CIM is rounded off as $R(B_iB_j - CA_{ij})$ with $R = 1/2$. By performing simulated annealing [43] calculations without round off, we confirmed that an error caused by this rounding is not critical to the GS search.

Actual computational time

The Ising-solver process of the CIM is completed in 500 μs, which is the time for 100 round trips of DOPO pulses in the 1-km cavity. The obtained spin configurations are stored in the FPGA module and transferred to the CPU for updating the interaction matrix of the next stage. The calculations in the digital part take at most 30 μs when the feedback algorithms are used. Since the current FPGA module uses a slow serial communication interface (RS-232C), it takes a few seconds to transfer the annealing results and the updated matrix between the FPGA module and the CPU. Although this technical issue is beyond the current scope, it is important to discuss how much we can shorten the transfer time.

For example, by using 10 Gigabit Ethernet (10 Gbps), the transfer time for $J_{ij}^{(l)}$ consisting of 8×512^2 bits is estimated to be 0.2 ms ideally. Note that $J_{ij}^{(l)}$ can be written as $J_{ij}^{(l)} = W_{ij}^{(l)} J_{ij}$ with $W_{ij}^{(l+1)} \equiv \delta(S_i^{(l)}, S_j^{(l)})$. Except for the first stage, it is enough to transfer $S_i^{(l)}$ of $\log_2 M \times 512$ bits in a few μs. Furthermore, we can directly write the $J_{ij}^{(l)}$-update logic in an FPGA module, which does not take any time to data transfer except for the first input and final output. System-on-chip (SoC) FPGA devices may be used to implement rather complicated feedback algorithms.

Comparison with other algorithms

We compared our experimental clustering results with other algorithms running on a standard CPU. We used reliable algorithms [43,44], i.e., the Louvain greedy [33] and Infomap algorithms [34]. The greedy algorithm reached the same best solution of $Q = 0.646$ with a small rate (about 2%), and it frequently reached the second and third best solution with $Q \sim 0.643$ (over 70%). The Infomap algorithm reached the best solution with highest probability of about 60%. (See Supplementary Note 6 in SI for detailed results.) Louvain ran in about a few milliseconds, while Infomap took about a few seconds on an Intel(R) Xeon(R) CPU E5-2697 v2 @ 2.70GHz. However, the number of nodes was too small to evaluate the run times of these algorithms. A further benchmark study, e.g., like the one in Ref. [43], will be left to future work, because the number of nodes is strictly limited in the current setup.

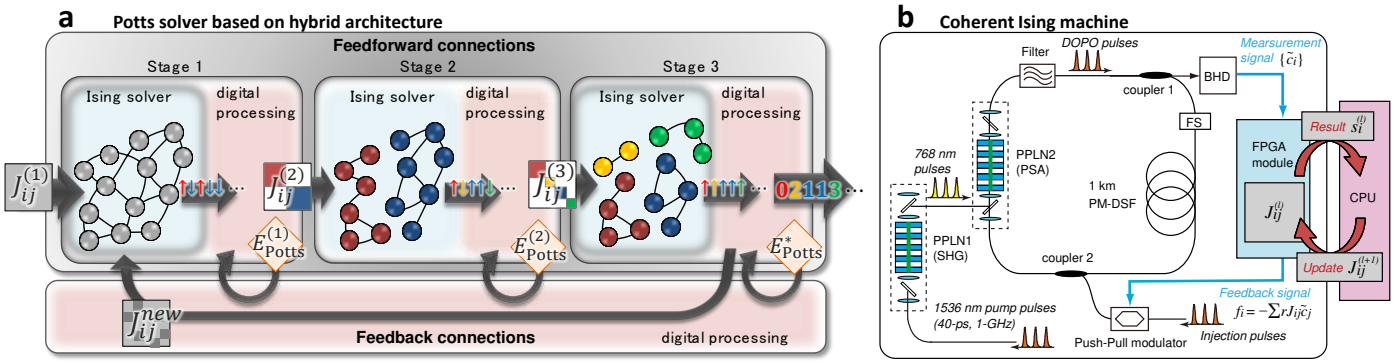

Fig. 1: Schematic view of a Potts-model solver and experimental setup of a CIM.
a, Potts-model solver composed of the hybrid architecture of iterated physical Ising-model solver and digital processed update of interaction matrix $J_{ij}^{(l)}$. The Ising solver sends a solution (set of up or down spins) to digital processing that computes the next interactions $J_{ij}^{(l+1)}$. In each iterative stage, the graph is divided into disconnected subgraphs and the interaction matrix becomes block diagonal. The nodes in each subgraph belong to a certain group (color) described by a multivalued spin. Digital processing can be used to implement various feedback algorithms to decrease the Potts energy $E_{\mathrm{Potts}}^{(l)}$ as discussed in the main text. **b,** Experimental setup of a coherent Ising machine (CIM). 512 degenerate optical parametric oscillators (DOPOs) in a 1-km-long fiber ring cavity are mutually coupled with J_{ij} through a measurement-feedback scheme assisted by an FPGA module. The solution of the l-th CIM computation is transferred to the CPU, and the updated $J_{ij}^{(l+1)}$ is embedded in the CIM again. The CIM (CPU) computation takes 500 μs (at most 30 μs) in each stage. PPLN: periodically poled lithium niobate, SHG: second harmonic generation, PSA: phase sensitive amplifier, FS: piezo-based fiber stretcher, PM-DSF: polarization-maintained dispersion shifted fiber, BHD: balanced homodyne detection.

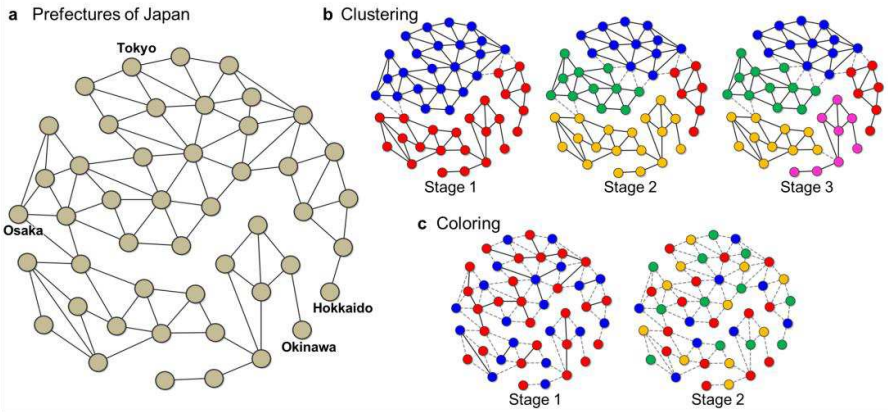

Fig. 2: Graph structure of the problem solved in this study and the best solutions found in each stage of experiments.
a, Graph of prefectures in Japan, where the number of nodes and edges are 47 and 92, respectively. **b,** One of the solutions obtained in each stage of graph clustering based on modularity. The dotted lines are the reduced edges in each stage. In the third stage, prefectures in Japan are grouped into five regions with a modularity of 0.646, which is the same as the best solution obtained by the other algorithms. **c,** One of the successful solutions of the four-color map problem. In stage two, there are no adjacent same-color nodes.

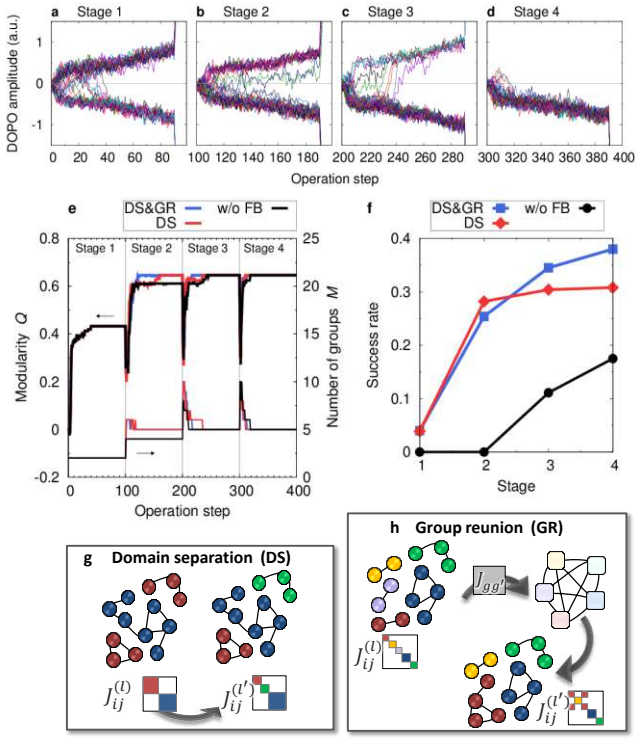

Fig. 3: Experimental results for graph clustering, and illustration of feedback algorithms.
a-d, DOPO amplitudes of 47 nodes as a function of operation step at stage $l = 1,2,3,4$. Positive (negative) amplitudes represent up (down) Ising spins. Crossover from antiferromagnetic to ferromagnetic solutions is found as l increases. **e,** Modularity Q and number of groups M without feedback (w/o FB) (thick and thin black lines, respectively) and those with domain separation (DS) algorithm (red lines) and both group reunion (GR) and DS algorithms (blue lines). **f,** Success rate of reaching the highest $Q(= 0.646)$ as estimated by sampling 1000 trials. **g-h,** Schematic view of DS and GR feedback algorithms.

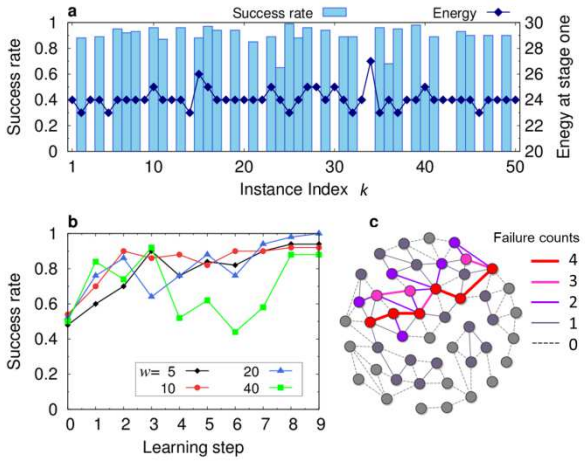

Fig. 4: Experimental results for map coloring problem with four colors.
a, Conditional success rates for 50 instances of $J_{ij,k}^{(2)}$ in stage two with $k = 1, 2, \ldots, 50$, and the Potts energy in stage one $E_{\mathrm{Potts},k}^{(1)}$. Total success rate averaged over k is about 50%. **b,** Change in success rates caused by learning defined as $J_{ij}^{\mathrm{new}} = J_{ij}^{\mathrm{old}} + w\,L_{ij}$ for weights $w = 5, 10, 20,$ and 40 with initial weight $w_0 = 40$. The matrix L_{ij} characterizes the edges that failed in coloring as detailed in the main text. **c,** The total number of mistakes (sum of L_{ij}) in independent learning processes with $w = 5, 10, 20,$ and 40. Red nodes and edges were frequently involved in the mistakes. Success rates can be improved by learning such frequently incorrect edges.

References:

1. Barahona, F. On the computational complexity of Ising spin glass models. *J. Phys. A* **15**, 3241–3253 (1982).

2. Kim, K. et al. Quantum simulation of frustrated Ising spins with trapped ions. *Nature* **465**, 590–593 (2010).

3. Simon, J., et al. Quantum simulation of antiferromagnetic spin chains in an optical lattice. *Nature* **472**, 307-312 (2011)

4. Johnson, M. W. et al. Quantum annealing with manufactured spins. *Nature* **473**, 194–198 (2011).

5. Marandi, A., Wang Z., Takata, K., Byer, R. L., Yamamoto, Y., Network of time-multiplexed optical parametric oscillators as a coherent Ising machine. *Nat. Photonics* **8**, 937–942 (2014).

6. Yamaoka, M. et al., 20k-spin Ising chip for combinatorial optimization problem with CMOS annealing. *Proc. Inter. Solid-State Circ. Conf.* **24** 3 (2015).

7. Mahboob, I., Okamoto, H., and Yamaguchi, H., An electromechanical Ising Hamiltonian. *Science Advances* **2**, e1600236 (2016).

8. Tsukamoto, S., Takatsu, M., Matsubara, S., and Tamura, H., An accelerator architecture for combinatorial optimization problems. FUJITSU Sci. Tech. J **53**, 8-13 (2017).

9. Sutton, B., Camsari, K. Y., Behin-Aein, B., and Datta, S., Intrinsic optimization using stochastic nanomagnets. *Scientific Reports* **7** (2017).

10. Inagaki, T. et al, A coherent Ising machine for 2000-node optimization problems, *Science* **354**, 603—606 (2016).

11. Denchev, V. S., et al, What is the Computational Value of Finite-Range Tunneling? *Phys. Rev. X* **6**, 031015 (2016)

12. Ronnow, T. F. et al., Defining and detecting quantum speedup. *Science* **345**, 420-424 (2014).

13. Boixo, S., et al, Computational Multiqubit Tunnelling in Programmable Quantum Annealers, *Nat. Commun.* **7**, 10327 (2016).

14. Parihar, A., Shukla, N., Jerry, M., Datta, S., and Raychowdhury, A. Vertex coloring of graphs via phase dynamics of coupled oscillatory networks. *Scientific reports* **7**, 911 (2017).

15. Sakaguchi, H., et al, Community detection by laser network dynamics. *J. Phys. Commun.* **2** 015005 (2018)

16. Yin, X. et al., Efficient analog circuits for boolean satisfiability. *IEEE Transactions on Very Large Scale Integration (VLSI) Systems* **26**, 155--167 (2018).

18. Wu, F. Y., The Potts model. *Reviews of Modern Physics*, **54**, 235 (1982)

19. Essam, J. W., Percolation theory., *Rep. Prog. Phys.* **43** 833 (1980)

20. Lucas, A., Ising formulations of many NP problems. *Frontiers in Physics* **2**, 5 (2014),

21. Narimani, A., et al, Combinatorial Optimization by Decomposition on Hybrid CPU–non-CPU Solver Architectures. *arXiv:1708.03439*

22. D-Wave Hybrid Solver Service: An Overview. D-Wave Technical Report 14-1039A-A (2020).

23. Utsunomiya, S., Takata, K., and Yamamoto, Y., Mapping of Ising models onto injection-locked laser systems. *Opt. Express* **19**, 18091–18108 (2011).

24. Inagaki, T., et al, Large-scale Ising spin network based on degenerate optical parametric oscillators. *Nat. Photonics* **10**, 415–419 (2016).

25. McMahon, P. L. et al., A fully-programmable 100-spin coherent Ising machine with all-to-all connections. *Science* **354**, 614--617 (2016).

26. Fortunato, S., Community detection in graphs. *Physics Reports* **486** (2010) 75–174

27. Schwarz A. J., et al. Community structure and modularity in networks of correlated brain activity, *Magn. Reson. Imag.* **26** 914-920 (2008)

28. Viana M. P., et al. Modularity and robustness of bone networks, *Mol. Biosyst.* **5** 255-261 (2009)

29. Newman, M. E. J., and Girvan, M., Finding and evaluating community structure in networks. *Phys. Rev. E* **69**, 026113 (2004)

30. Reichardt, J., and Bornholdt, S., Statistical mechanics of community detection. *Phys. Rev. E* **74**, 016110 (2006)

31. Ronhovde, P., and Nussinov, Z., Multiresolution community detection for megascale networks by information-based replica correlations. *Phys. Rev. E* **80**, 016109 (2009).

32. Hameley, R. et al, Experimental investigation of performance differences between Coherent Ising Machines and a quantum annealer. *arXiv:1805.05217*

33. Blondel, V. D., et al, Fast unfolding of communities in large networks. *Journal of Statistical Mechanics: Theory and Experiment* **10**, P1000 (2008);
https://sites.google.com/site/findcommunities/

34. Rosvall, M., and Bergstrom, C. T., Maps of random walks on complex networks reveal community structure. *PNAS* **105**, 1118-1123 (2008);
http://www.mapequation.org/code.html

35. Appel, K., and Haken, W., Every map is four colorable. *Bulletin of the American Mathematical Society* **82** (1976), 711–712

36. Lewis, R., A Guide to Graph Colouring: Algorithms and Applications. *Springer International Publishers,* (2015)

37. Marx, Dániel (2004), Graph colouring problems and their applications in scheduling, Periodica Polytechnica, Electrical Engineering, 48 (1–2),

38. Rosenhouse, J., and Taalman, L., Taking Sudoku Seriously: The Math Behind the World's Most Popular Pencil Puzzle. *Oxford University Press* (2012)

39. King, D., et al. Emulating the coherent Ising machine with a mean-field algorithm. *arXiv:1806.08422*

40. Tiunov, E. S., Ulanov, A. E., and Lvovsky, A. I., Annealing by simulating the coherent Ising machine. *arXiv:1901.08927*

41. M. E. Marhic, C. H. Hsia, J. M. Jeong, Optical amplification in a nonlinear fiber interferometer. Electron. Lett. 27, 210-211 (1991).

42. R.-D. Li, P. Kumar, W. L. Kath, Dispersion compensation with phase-sensitive optical amplifiers. J. Lightwave Technol. 12, 541–549 (1994).

43. Kirkpatrick, S., Gelatt Jr, C. D., and Vecchi, M. P., Optimization by Simulated Annealing. *Science* **220,** 671–680 (1983)

43. Lancichinetti, A., and Fortunato S, Community detection algorithms: A comparative analysis. *Phys. Rev. E* **80,** 056117 (2009).

44. Danon, L. et al, Comparing community structure identification. *J. Stat. Mech.* P09008 (2005)

Figures

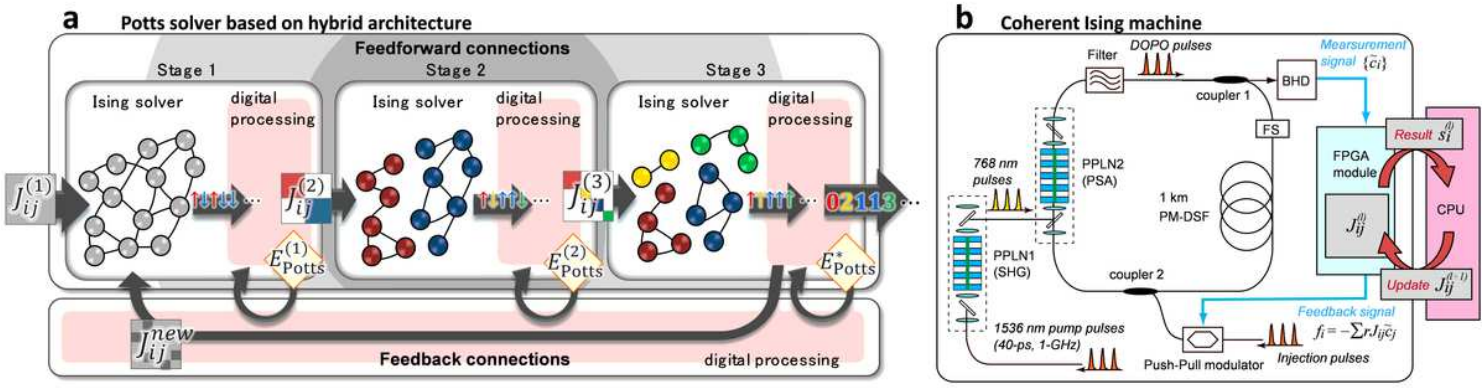

Figure 1

Schematic view of a Potts-model solver and experimental setup of a CIM. [See manuscript PDF file for full caption]

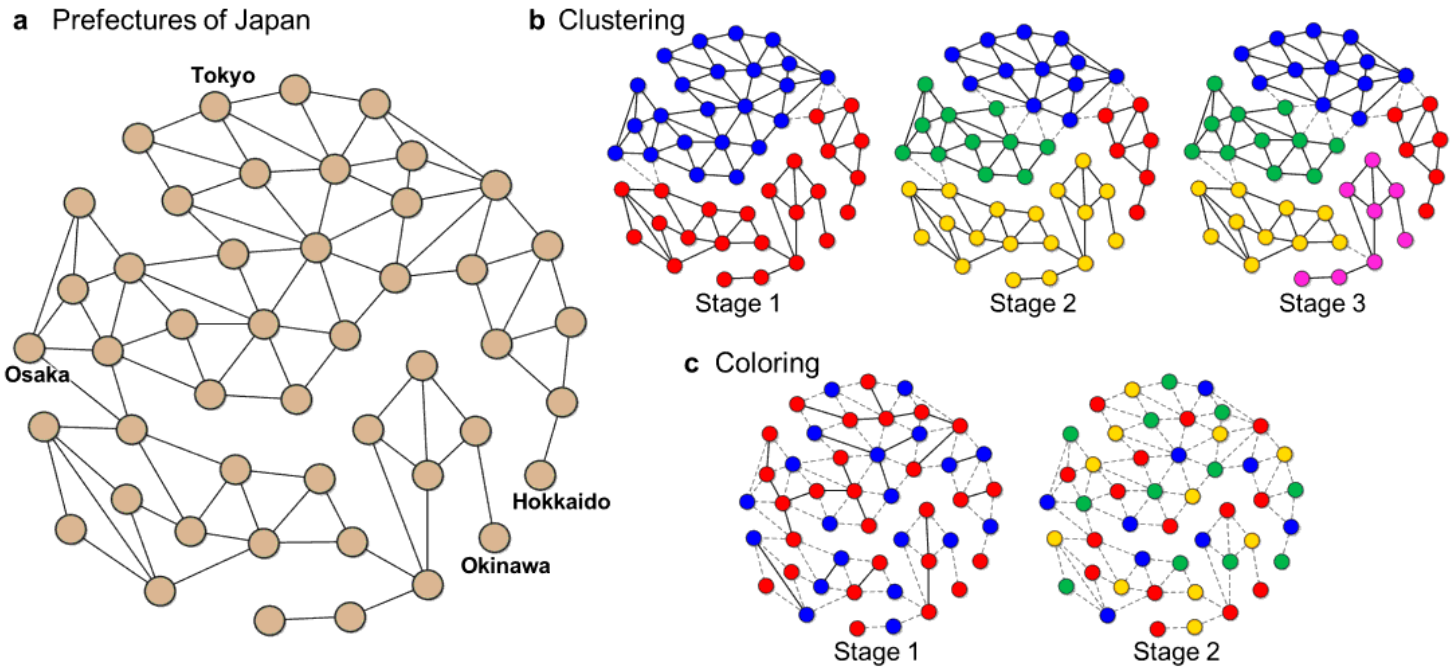

Figure 2

Graph structure of the problem solved in this study and the best solutions found in each stage of experiments. a, Graph of prefectures in Japan, where the number of nodes and edges are 47 and 92, respectively. b, One of the solutions obtained in each stage of graph clustering based on modularity. The dotted lines are the reduced edges in each stage. In the third stage, prefectures in Japan are grouped into five regions with a modularity of 0.646, which is the same as the best solution obtained by the other algorithms. c, One of the successful solutions of the four-color map problem. In stage two, there are no adjacent same-color nodes.

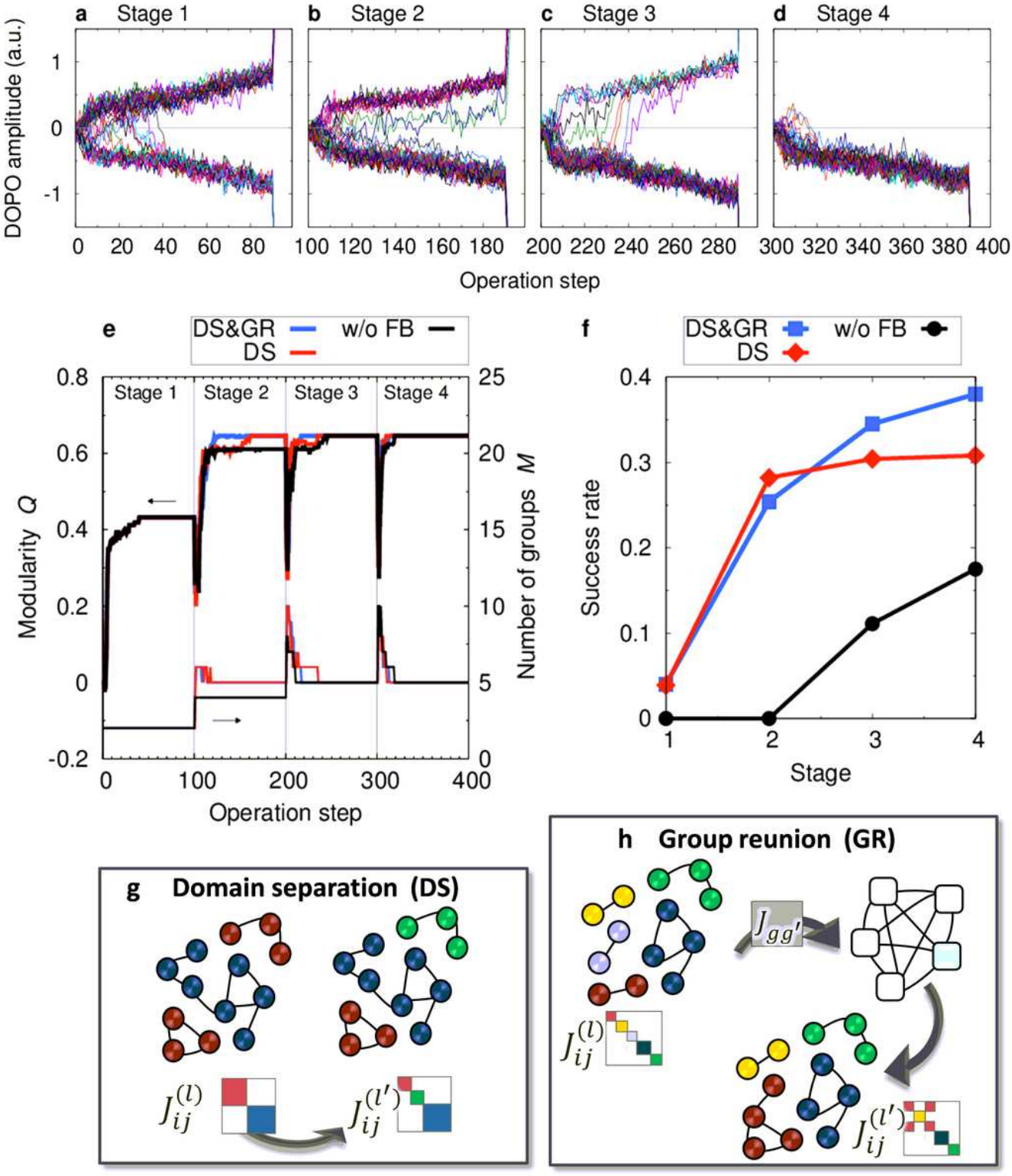

Figure 3

Experimental results for graph clustering, and illustration of feedback algorithms. [See manuscript PDF file for full caption]

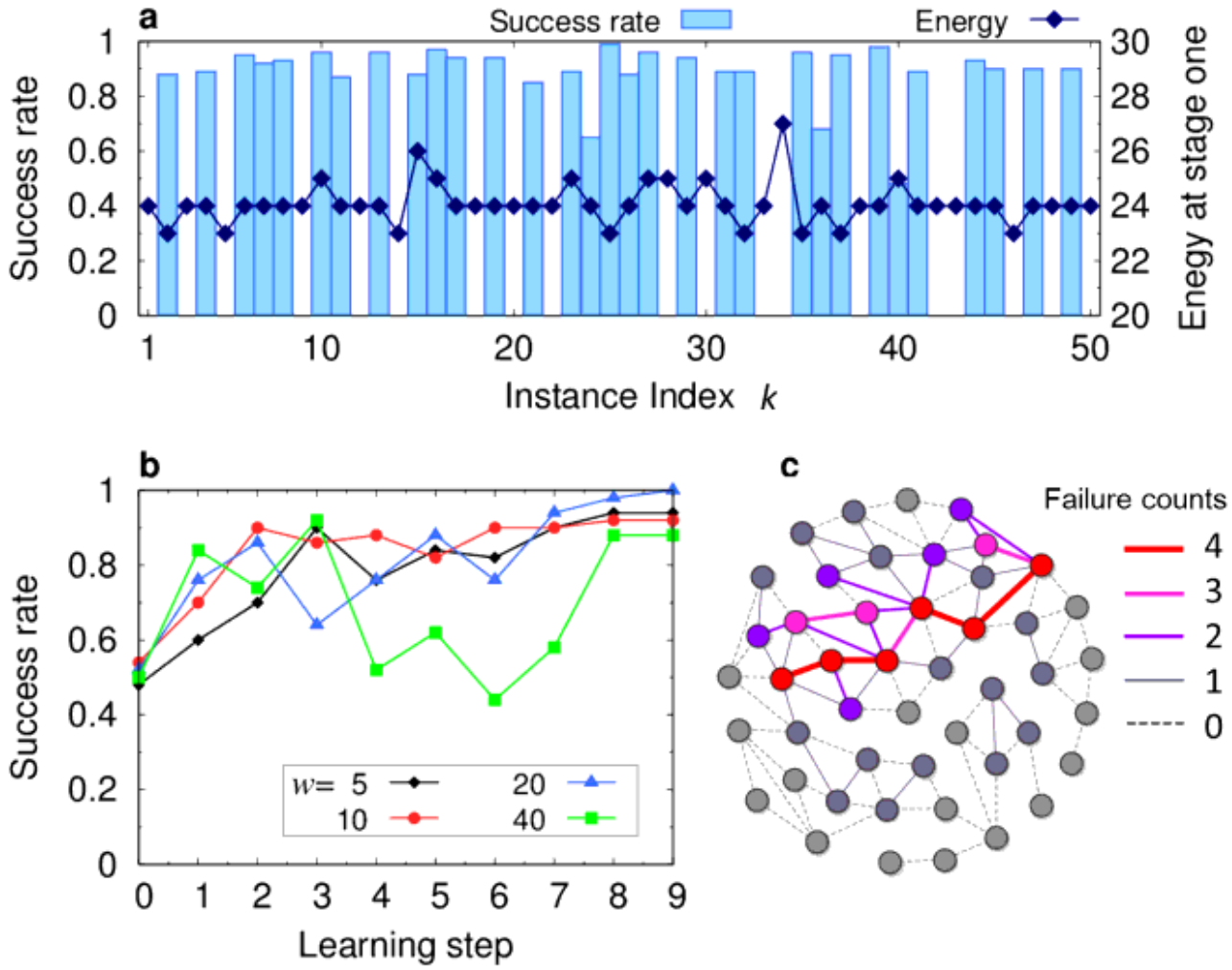

Figure 4

Experimental results for map coloring problem with four colors. [See manuscript PDF file for full caption]

Supplementary Files

This is a list of supplementary files associated with this preprint. Click to download.

- Supplementaryv020.docx